

# Optical and transport properties of spheroidal metal nanoparticles with account for the surface effect

Nicolas I. Grigorchuk\*

*Bogolyubov Institute for Theoretical Physics, National Academy of Sciences of Ukraine, 14-b Metrologichna Strasse, Kiev-143, 03680, Ukraine*

Petro M. Tomchuk†

*Institute for Physics, National Academy of Sciences of Ukraine, 46, Nauky Avenue, Kiev-28, 03680, Ukraine*

(Received 23 March 2011; revised manuscript received 30 May 2011; published 30 August 2011)

The kinetic approach is applied to develop the Drude-Sommerfeld model for studying the optical and electrical transport properties of spheroidal metallic nanoparticles when the free electron path is much greater than the particle size. For the nanoparticles of an oblate or a prolate spheroidal shape a dependence of the dielectric function and the electric conductivity on a number of factors, including the frequency, the particle radius, the spheroidal aspect ratio, and the orientation of the electric field with respect to the particle axes, has been found. The oscillations of the real and imaginary parts of the dielectric permeability have been found with increasing particle size at some fixed frequencies or with frequency increasing at some fixed radius of a nanoparticle. The results obtained in the kinetic approach are compared with those known from the classical model.

DOI: [10.1103/PhysRevB.84.085448](https://doi.org/10.1103/PhysRevB.84.085448)

PACS number(s): 78.67.Bf, 68.49.Jk, 73.23.-b

## I. INTRODUCTION

Understanding how light interacts with matter at the nanometer scale is a fundamental problem in nanophotonics and optoelectronics. The variety of applications is based on the surface-bound optical excitations in metallic nanoparticles (MNs). They include plasmonic nanomaterials, optical nanosensors, biomarkers, integrated circuits, and subwavelength waveguides, molecular imaging, metamaterials with a negative refractive index, optical antennas, and so on (see, e.g., Refs. 1–7).

The optical and transport properties of the MNs have been investigated for a long time, and the results have been presented quite completely in a number of reviews<sup>8–11</sup> and monographs,<sup>12–16</sup> especially for MNs of a spherical shape.

The dielectric function is the most important factor for the design and optimization of plasmon nanometer-sized structures. However, this function for MNs differs from an ideal bulk metal. The difference depends on many factors, such as the size and shape of the MNs and the surrounding media.<sup>18–22</sup> That is why the dielectric function of MNs has been under comprehensive study for many years.<sup>12–17</sup> The size effect becomes more significant when the size  $d$  of MN is comparable with the electron mean free path  $l$ . The ratio between  $d$  and  $l$  is a very important physical characteristic, which eventually defines the mechanism of an electron relaxation rate inside the MN. As a rule, the cases  $d \gg l$  and/or  $d \ll l$  are studied. The former case refers to the so-called diffusive electron dynamics, and the latter one refers to the ballistic electron dynamics. The diffusive case has been studied in detail since it enables us to use the Mie theory for a uniform media<sup>23</sup> or the Maxwell-Garnett theory<sup>24</sup> for a composite media in the calculations of the optical properties of the MN.

In particular, when  $d \gg l$ , the following expression for dielectric permeability that results from the Drude-Sommerfeld

theory<sup>16,25</sup> has been often used:

$$\epsilon(\omega) = \epsilon'(\omega) + i\epsilon''(\omega) = 1 - \frac{\omega_{pl}^2}{v^2 + \omega^2} + i\frac{v}{\omega} \frac{\omega_{pl}^2}{v^2 + \omega^2}. \quad (1)$$

Here  $v$  is the collision frequency inside the particle bulk,  $\omega_{pl} = \sqrt{4\pi ne^2/m}$  is the frequency of plasma electrons oscillations in the metal,  $e$  and  $m$  are the electron charge and mass, respectively, and  $n$  is the electron concentration. The imaginary part of the dielectric permeability  $\epsilon''(\omega)$  is connected to the high-frequency (optical) conductivity by the well-known relation

$$\sigma(\omega) = \frac{\omega}{4\pi} \epsilon''(\omega) = \frac{v}{4\pi} \frac{\omega_{pl}^2}{v^2 + \omega^2}. \quad (2)$$

For sufficiently low frequencies ( $\omega \rightarrow 0$ ), one gets the expression  $\sigma_0 = ne^2/mv$ , describing the static conductivity.

In the case when the sizes of the MN are less than the mean electronic free path in the particle, the mechanism of electron scattering is changed, and the surface of the particle starts to play a dominate role. This effect will be called the surface or boundary effect. Strictly speaking, in this case neither Mie nor Drude-Sommerfeld theory can be applied, and another approach ought to be elaborated to present the optical properties of MNs. As has been shown,<sup>26,27</sup> a clear size dependence of relaxation dynamics is observed in experiments. This is a strong indication of an efficient electron-surface phonon interaction in this regime. But the experimental results<sup>18,28–33</sup> are often analyzed within the frame of the named theories, or to simplify the problem, Eqs. (1) and (2) have been used with formal replacements<sup>15,33–35</sup>

$$v \rightarrow \frac{3}{4} \frac{v_F}{R} \quad \text{or} \quad v \rightarrow A v_F \frac{S}{4V}, \quad (3)$$

where  $v_F$  is the electron velocity at the Fermi surface,  $R$  refers to the particle radius,  $V$  and  $S$  refer to the volume and the surface area of the spherical particle, respectively, and  $A$  is a coefficient obtained by fitting the calculations to the

experimental data. In other words, the collision frequency in the particle volume is replaced by some effective collision frequency. But such a replacement can be applied for the MNs of a spherical shape only. If the geometry of MN differs from the spherical one and the condition  $d \ll l$  holds for at least one of the particle directions, then the optical conductivity becomes the tensor quantity,<sup>21</sup> and the formal replacement similar to the one presented by Eq. (3) can no longer be used. It is necessary to look more closely at the effect of the particle boundaries on the optical properties. For a theoretical study it is convenient to choose a particle with a spheroidal shape. That is because the results obtained for particles with such a shape can be easily extended to particles with other shapes by means of the formal transformation of the spheroidal axes.

Thus, there arises a problem in the case  $d \ll l$  of how to calculate the values of  $\epsilon$  or  $\sigma$  when the above-mentioned classical models cannot be used.

The present work is devoted to the elaboration of the new approach, allowing us to calculate the real and imaginary parts of the dielectric permeability for MNs of a spheroidal shape in the case when the inequality  $d \ll l$  holds.

Since both the real and the imaginary parts of  $\epsilon(\omega)$  govern the numerous properties of the MNs, the necessity of the detailed study of the boundary effect on the dielectric permeability has become evident.

The rest of the paper is organized as follows. The kinetic approach to the problem is presented in Sec. II. Section III contains the study of the conductivity in the spheroidal MNs. In Sec. IV, we consider the limit cases of the problem and the size effects. Section V is devoted to the discussion of the obtained results, and Sec. VI contains the conclusions.

## II. KINETIC EQUATION METHOD

To account for the effect of MN boundaries on the optical and electrical transport properties of the MN, we will apply the kinetic equations approach. The advantage of this approach is that the obtained results can be applied to strongly anisotropic spheroidal (needle-like or disk-shaped) MNs, but in the case of MNs with a spherical shape it transforms to the well-known results,<sup>16,25</sup> such as the ones given by Eqs. (1) and (2). Thus, it permits one to study the effect of the particle shape on the measured physical values. Second, the kinetic method enables us to investigate the MNs with sizes greater or less than the electron mean free path  $l$ . But there exists a lower limit of the applicability of this method in the small radius limit when the particle size is comparable to the de Broglie wavelength of the electron, and the quantization of the electron spectrum starts to play an essential role.<sup>36–38</sup> Practically, it is around a radius of greater or less than 2 nm. Beyond the electronic Fermi distribution function, the influence of quantum effects on the optical conductivity can manifest itself in the quantization of electron pulses and angular momentums. It is important at low temperatures, when the distance between successive energy levels is much higher than  $k_B T$ .

Let us consider the single MN that is irradiated by an electromagnetic wave, whose electric field is given as

$$\mathbf{E} = \mathbf{E}_0 \exp[i(\mathbf{k}\mathbf{r} - \omega t)]. \quad (4)$$

Here  $\mathbf{E}_0$  is the amplitude of an electric field,  $\omega$  is its frequency,  $\mathbf{k}$  is the wave vector, and  $\mathbf{r}$  and  $t$  describe the spatial coordinates and time.

We will assume that the electromagnetic wave length is far above the particle size. If one chooses the coordinate origin in the center of the particle, then the above-mentioned assumption is written as

$$kr \ll 1. \quad (5)$$

The inequality (5) implies that the  $\mathbf{E}$  field of the electromagnetic wave can be considered to be spatially uniform on scales of the order of a particle size. This means that the field represented by Eq. (4) induces inside of the MN an electric field that is varying in time but uniform in space. The amplitude of such a field is connected to  $\mathbf{E}_0$  by the relation<sup>39</sup>

$$E_{\text{in}}^j(\omega) = \frac{E_0^j(0, \omega)}{1 + L_j[\epsilon(\omega) - 1]}, \quad (6)$$

where  $L_j$  are depolarization factors in the  $j$ th direction (in the principal axes of an ellipsoid). The explicit expressions of  $L_j$  for a single MN of an ellipsoidal shape can be found elsewhere (see, e.g., Refs. 40 and 41).

The field  $E_{\text{in}}$  has an effect on the equilibrium electron velocity distribution and thus determines the appearance of a nonequilibrium addition  $f_1(\mathbf{r}, \mathbf{v}, t)$  to the Fermi distribution function  $f_0(\epsilon)$ . Here  $\epsilon = m v^2/2$  is the kinetic energy of an electron, and  $v = |\mathbf{v}|$  refers to the electron velocity. As is well known,<sup>42</sup> the equilibrium function  $f_0(\epsilon)$  does not give any input to the current. Accounting for both the time dependence of Eq. (4) and the inequality (5), the distribution function of electrons, which generates the field  $E_{\text{in}}$ , can be written as

$$f(\mathbf{r}, \mathbf{v}, t) = f_0(\epsilon) + f_1(\mathbf{r}, \mathbf{v}, t) \equiv f_0(\epsilon) + f_1(\mathbf{r}, \mathbf{v}) e^{i\omega t}. \quad (7)$$

The function  $f_1(\mathbf{r}, \mathbf{v})$  can be found as a solution of the linearized Boltzmann's equation

$$(v - i\omega)f_1(\mathbf{r}, \mathbf{v}) + \mathbf{v} \cdot \frac{\partial f_1(\mathbf{r}, \mathbf{v})}{\partial \mathbf{r}} + e \mathbf{E}_{\text{in}} \mathbf{v} \cdot \frac{\partial f_0(\epsilon)}{\partial \epsilon} = 0. \quad (8)$$

In Eq. (8) we have assumed that the collision integral  $(\partial f_1 / \partial t)_{\text{col}} = -f_1 / \tau$  is evaluated in the relaxation time approximation ( $\tau = 1/\nu$ ). What is more, the function  $f_1(\mathbf{r}, \mathbf{v})$  ought to satisfy the boundary conditions as well. These conditions may be chosen from the character of electron reflection from the inner walls of the MN. We will take, as is usually done, the assumption of diffusive electron scattering by the boundary of MN. Placing the origin of the coordinates at the center of the particle, we can present this boundary conditions in the form

$$f(\mathbf{r}, \mathbf{v})|_S = 0, \quad \mathbf{v}_n < 0, \quad (9)$$

where  $\mathbf{v}_n$  is the velocity of the component normal to the particle surface.

Along with diffusive scattering, the mirror boundary conditions at the nanoparticle surface were examined in the literature for electron scattering (see, e.g., Refs. 42 and 43). In this case, each electron is reflected from the surface at the same angle at which it falls to the surface. In diffuse reflection, the electron is reflected from the surface at any angle. In order for the mirror mechanism to be dominant, the surface must be perfectly

smooth in the atomic scale since the degree of reflectivity of the boundary essentially depends on its smoothness. Practically, for a nonplanar border such smoothness is extremely difficult to achieve. As was shown,<sup>43</sup> the mirror boundary conditions give a small correction to the results obtained with the account of only the diffusive electron reflections. Therefore, we chose more realistic boundary conditions given by Eq. (9).

It is comparatively easy to solve Eq. (8) and to satisfy the boundary conditions of Eq. (9) if one passes to the transformed coordinate system, where an ellipsoid with semiaxes  $R_1, R_2, R_3$  transforms into a sphere of radius  $R$  with the same total volume:

$$x_j = \frac{R_j}{R} x'_j, \quad R = (R_1 R_2 R_3)^{1/3}. \quad (10)$$

A similar transformation should be made for the electron velocities as well:  $v_j = v'_j R_j / R$ . Then, solving Eq. (8), one finds

$$f_1(\mathbf{r}, \mathbf{v}, t) = -e \frac{\partial f_0}{\partial \varepsilon} \mathbf{v} \mathbf{E}_{\text{in}} \frac{1 - \exp[-(v - i\omega) t'(\mathbf{r}', \mathbf{v}')] ]}{v - i\omega}, \quad (11)$$

where the characteristic of Eq. (8) can be presented as

$$t' = \frac{1}{v^2} [\mathbf{r}' \mathbf{v}' + \sqrt{(\mathbf{R}^2 - \mathbf{r}'^2) \mathbf{v}'^2 + (\mathbf{r}' \mathbf{v}')^2}]. \quad (12)$$

The characteristic curve of Eq. (12) depends only on the absolute value of  $\mathbf{R}$  and does not depend on the direction of  $\mathbf{R}$ . The radius vector  $\mathbf{R}$  determines the starting position of an electron at the moment  $t' = 0$ .

Generally speaking, the presence of the surface changes both the current and the field distributions. It is reasonable to point out here that, though the electric field still remains homogeneous inside of the MN [in accordance with Eq. (5)], the distribution function  $f_1$  in any case depends on coordinate due to the necessity to meet the boundary condition given by Eq. (9).

Performing the Fourier transformation of Eq. (11), one can calculate the density of a high-frequency current induced by the electromagnetic wave of Eq. (4) inside the MN via the expression

$$\mathbf{j}(\mathbf{r}, \omega) = 2e \left( \frac{m}{2\pi\hbar} \right)^3 \iiint \mathbf{v} f_1(\mathbf{r}, \mathbf{v}, \omega) d^3v. \quad (13)$$

Let us introduce the tensor of the complex conductivity  $\sigma_{\alpha\beta}^c(\mathbf{r}, \omega)$  using the relationship

$$j_\alpha(\mathbf{r}, \omega) = \sum_{\beta=1}^3 \sigma_{\alpha\beta}^c(\mathbf{r}, \omega) E_{\text{in}}^\beta. \quad (14)$$

Then in accordance with both Eqs. (11) and (13), the components of this tensor can be presented in the form

$$\begin{aligned} \sigma_{\alpha\beta}^c(\mathbf{r}, \omega) = & 2e \left( \frac{m}{2\pi\hbar} \right)^3 \iiint v_\alpha \left[ -e v_\beta \frac{\partial f_0}{\partial \varepsilon} \right. \\ & \left. \times \left( \frac{1 - e^{-(v-i\omega)t'(r', v')}}{v - i\omega} \right) \right] d^3v. \end{aligned} \quad (15)$$

Before beginning a detailed study of the role of the particle surface and the size effects, which will be given below, it is worth noting here the following. The surface effect on the conducting phenomenon is described in Eq. (15) by means

of the characteristic  $t'(\mathbf{r}', \mathbf{v}')$ . It accounts for the restrictions imposed on the electron movement by a nanoparticle surface. As one can see from Eq. (12), the value of  $t'$  is of the order of  $t' \sim R/v_F$ , where  $v_F$  is the Fermi velocity. This implies that the value reciprocal to  $t'$  will correspond to the vibration frequency between the particle walls. Hence, the inequality  $v t' \gg 1$  indicates that the electron collision frequency inside the volume of MN would significantly exceed the one for an electron collision with the surface of MN. If described inequality is satisfied, it is possible to direct  $t' \rightarrow \infty$ , and the exponent in Eq. (15) can be neglected. Then, we obtain a standard expression for the dielectric permeability, such as given in Eq. (2). To ensure that, it is necessary to pass in Eq. (15) to the integration over  $v$  in the spherical coordinate system

$$\iiint_{-\infty}^{\infty} d^3v \rightarrow \int_0^{2\pi} d\varphi \int_0^\pi \sin\theta d\theta \int_0^\infty v^2 dv,$$

with the use of the formulas

$$\int_0^\infty v^4 \delta(v^2 - v_F^2) dv = \frac{v_F^3}{2}, \quad (16)$$

$$n = \frac{8\pi}{3} \left( \frac{m v_F}{2\pi\hbar} \right)^3, \quad (17)$$

and to take into account that the energy derivative of  $f_0$  in the zero approximation in the small ratio of  $k_B T / \varepsilon_F$  can be replaced by

$$\frac{\partial f_0}{\partial \varepsilon} \approx -\delta(\varepsilon - \varepsilon_F), \quad (18)$$

as well as the fact that only the diagonal terms with  $v_\alpha = v_\beta = v$  are retained after integration over all angles.

At the end of this section, we would like to pay attention to the next two important circumstances. (i) Though the inner field  $\mathbf{E}_{\text{in}}$  is spatially uniform, the distribution function  $f_1(\mathbf{r}, \mathbf{v}, \omega)$  and, consequently, the density of the current  $\mathbf{j}(\mathbf{r}, \omega)$  are dependent on the coordinates. This dependence is imposed by the boundary conditions of Eq. (9). (ii) The density of the current and the components of the conductivity tensor have the physical sense only if they are averaged over the particle volume. For instance, it is easy to ensure that the energy absorbed by a single MN is determined either by an averaged density of the current  $\langle j \rangle$  or by an averaged tensor of the complex conductivity  $\langle \sigma_{\alpha\beta}^c(\mathbf{r}, \omega) \rangle$  [accounting for Eq. (14)].

### III. CONDUCTIVITY OF SPHEROIDAL METALLIC NANOPARTICLES

Let us average over coordinates the components of the conductivity complex tensor represented by Eq. (15). The necessity of such an averaging arises from the fact that the power absorbed by a single MN is caused by the conductivity averaged over the volume of MN. Then, in view of Eq. (18), one gets the expression

$$\begin{aligned} \langle \sigma_{\alpha\beta}^c(\mathbf{r}, \omega) \rangle = & \frac{4e^2}{m} \left( \frac{m}{2\pi\hbar} \right)^3 \frac{1}{v - i\omega} \int \frac{d^3r'}{V} \\ & \times \int d^3v v_\alpha v_\beta \delta(v^2 - v_F^2) [1 - e^{(v-i\omega)t'}], \end{aligned} \quad (19)$$

where the angle brackets denote the averaging. First, we can fulfill the integration in Eq. (19) over all electron coordinates. In accordance with Ref. 39, one can find that

$$\frac{1}{V} \int d^3 r' [1 - e^{-(v-i\omega)t'(\mathbf{r}', \mathbf{v}')} ] = \frac{3}{4} \Psi(q), \quad (20)$$

where the following notations have been used:

$$\Psi(q) = \frac{4}{3} - \frac{2}{q} + \frac{4}{q^3} - \frac{4}{q^2} \left(1 + \frac{1}{q}\right) e^{-q}, \quad (21)$$

$$q = \frac{2R}{v'}(v - i\omega) \equiv q_1 - iq_2. \quad (22)$$

Further, we will take into account only the diagonal components of the conductivity tensor. Based on Eq. (20), we can rewrite Eq. (19) as

$$\langle \sigma_{\alpha\alpha}^c(\mathbf{r}, \omega) \rangle = \frac{3e^2 m^2}{(2\pi\hbar)^3} \frac{1}{v - i\omega} \int d^3 v v_\alpha^2 \delta(v^2 - v_F^2) \Psi(q). \quad (23)$$

Let us restrict ourselves only to the single MN of spheroidal shape. To calculate the residual integral, we pass to the spherical coordinate system with a  $z$  axis directed along the rotation axis of the spheroid (as we have done in the previous section) and take into account that the components of an electron velocity parallel ( $v_{\parallel}$ ) and perpendicular ( $v_{\perp}$ ) to this axis are defined as

$$v_{\parallel} = v_z = v \cos \theta, \quad v_{\perp} = \sqrt{v_x^2 + v_y^2} = v \sin \theta, \quad (24)$$

respectively, where

$$v_{(\perp)}^2 = v^2 \sin^2 \theta \begin{pmatrix} \cos^2 \varphi \\ \sin^2 \varphi \end{pmatrix}.$$

After integration in Eq. (23) over the azimuthal angle  $\varphi$  and over all electron velocities, in view of Eqs. (16) and (17), we obtain for the parallel and perpendicular components of the conductivity tensor the expressions

$$\sigma_{\parallel}^c \equiv \langle \sigma_{zz}^c(\mathbf{r}, \omega) \rangle = \frac{9 ne^2}{4 m} \frac{1}{v - i\omega} \int_0^{\pi/2} \sin \theta \cos^2 \theta \Psi(\theta) d\theta|_{v=v_F}, \quad (25)$$

and

$$\sigma_{\perp}^c \equiv \langle \sigma_{xx}^c(\mathbf{r}, \omega) \rangle = \langle \sigma_{yy}^c(\mathbf{r}, \omega) \rangle = \frac{9 ne^2}{8 m} \frac{1}{v - i\omega} \int_0^{\pi/2} \sin^3 \theta \Psi(\theta) d\theta|_{v=v_F}. \quad (26)$$

The subscript  $v = v_F$  means that the electron velocity in the final expressions should be taken on the Fermi surface. The  $\Psi$  function in Eqs. (25) and (26) varies now with the angle  $\theta$  because  $q$  [see Eq. (22)] for a spheroidal particle becomes dependent on the angle  $\theta$  and can be determined as

$$q = \frac{2}{v_F} \frac{v - i\omega}{\sqrt{\frac{\cos^2 \theta}{R_{\parallel}^2} + \frac{\sin^2 \theta}{R_{\perp}^2}}} \equiv q(\theta), \quad (27)$$

where  $R_{\parallel}$  and  $R_{\perp}$  are the semiaxes of the spheroid. Such a form for  $q$  follows from the form of “deformed” electron velocity, which enters into Eq. (22) and for a spheroid is

$$v' = vR \sqrt{\left(\frac{\sin \theta}{R_{\perp}}\right)^2 + \left(\frac{\cos \theta}{R_{\parallel}}\right)^2} \equiv v'(\theta), \quad (28)$$

where the velocity components  $v_{\parallel}$  and  $v_{\perp}$ , presented by Eq. (24), were used. The velocity  $v'$  does not depend on the particle radius  $R$  but depends only on the spheroid aspect ratio. In the case of a spherical particle  $R_{\parallel} = R_{\perp} \equiv R$ , and  $v' = v$ .

There is a well-known common relation<sup>42</sup> between the tensor components of the complex dielectric permeability and the components of a complex conductivity tensor:

$$\langle \epsilon_{\alpha\beta}(\mathbf{r}, \omega) \rangle = \delta_{\alpha\beta} + i \frac{4\pi}{\omega} \langle \sigma_{\alpha\beta}^c(\mathbf{r}, \omega) \rangle. \quad (29)$$

If one separates the real and the imaginary parts in the expressions for both the complex tensors of the dielectric permeability and the conductivity, i.e., presents

$$\langle \epsilon_{\alpha\beta}^c(\mathbf{r}, \omega) \rangle = \epsilon'_{\alpha\beta}(\omega) + i \epsilon''_{\alpha\beta}(\omega), \quad (30)$$

and

$$\langle \sigma_{\alpha\beta}^c(\mathbf{r}, \omega) \rangle = \sigma'_{\alpha\beta}(\omega) + i \sigma''_{\alpha\beta}(\omega), \quad (31)$$

then in correspondence to Eq. (29), one obtains

$$\epsilon'_{\alpha\beta}(\omega) = \delta_{\alpha\beta}(\omega) - \frac{4\pi}{\omega} \sigma''_{\alpha\beta}(\omega) \quad (32)$$

and

$$\epsilon''_{\alpha\beta}(\omega) = \frac{4\pi}{\omega} \sigma'_{\alpha\beta}(\omega). \quad (33)$$

Finally, using Eqs. (25), (26), and (31), one gets for a spheroidal particle

$$\begin{aligned} \sigma'_{(\parallel)}(\omega) &= \frac{9 ne^2}{4 m} \text{Re} \left[ \frac{1}{v - i\omega} \int_0^{\pi/2} \left( \frac{\sin \theta \cos^2 \theta}{\frac{1}{2} \sin^3 \theta} \right) \Psi(\theta) d\theta \right]_{v=v_F} \end{aligned} \quad (34)$$

and

$$\begin{aligned} \sigma''_{(\perp)}(\omega) &= \frac{9 ne^2}{4 m} \text{Im} \left[ \frac{1}{v - i\omega} \int_0^{\pi/2} \left( \frac{\sin \theta \cos^2 \theta}{\frac{1}{2} \sin^3 \theta} \right) \Psi(\theta) d\theta \right]_{v=v_F}. \end{aligned} \quad (35)$$

The upper (lower) symbols in the parentheses on the left-hand sides of Eqs. (34) and (35) correspond to the upper (lower) symbols in the parentheses on the right-hand sides of these equations. Formulas (34) and (35) are the fundamental equations for calculating the dielectric function and therefore for studying the optical properties of MNs.

For illustration, we present in Fig. 1 the frequency dependence of an imaginary part of the dielectric permeability ratio components for a spheroidal Au particle, which is obtained by numerical evaluating the integrals in Eqs. (33) and (34). It is worth noting that the radius  $R_{\parallel}$  is directed along the revolution axis of the spheroid, and  $R_{\perp}$  is transverse to it. These spheroidal

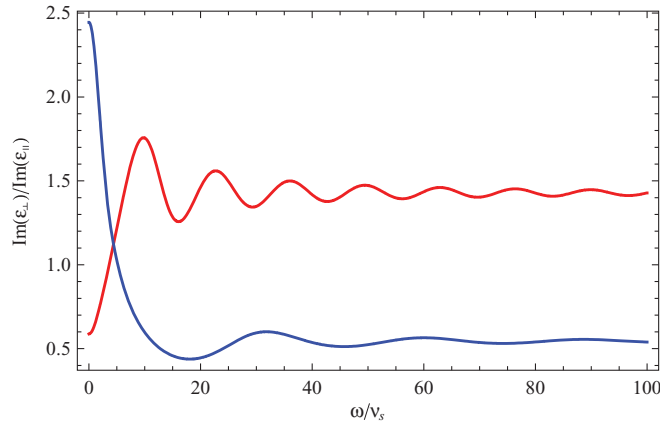


FIG. 1. (Color online) The dependence of the ratio  $\epsilon''_{\perp}/\epsilon''_{\parallel}$  for prolate ( $R_{\perp}/R_{\parallel} = 0.1$ , upper curve) and oblate ( $R_{\perp}/R_{\parallel} = 10$ , lower curve) Au particles (with  $R = 50 \text{ \AA}$ ) vs the frequency ratio  $\omega/\nu_s$ , where  $\nu_s = \nu_F/(2R)$ .

radii can be expressed through the radius of a sphere (of an equivalent volume) as

$$R = (R_{\parallel} R_{\perp}^2)^{1/3}.$$

The calculations were carried out using such parameters for Au:  $\nu = 3.39 \times 10^{13}$  at  $0^\circ\text{C}$  (Ref. 39),  $n = 5.9 \times 10^{22} \text{ cm}^{-3}$ ,  $\nu_F = 1.39 \times 10^8 \text{ cm/s}$  (Ref. 44).

As one can see, the ratio  $\epsilon''_{\perp}/\epsilon''_{\parallel}$  oscillates with increasing frequency both for the prolate and the oblate Au nanoparticles. These oscillations have a damping character for both prolate and oblate particles, but they differ in the period of oscillations. For a given prolate nanoparticle the oscillations occur around the constant value  $\epsilon''_{\perp}/\epsilon''_{\parallel} \simeq 4/3$ , and for oblate ones they occur in the vicinity of another constant,  $\epsilon''_{\perp}/\epsilon''_{\parallel} \simeq 1/2$ . The period of oscillations depends only slightly on the particle volume; however, the oscillation amplitude is more pronounced for particles with smaller radii.

It is also worth noting that the intensity of the surface mode is determined by the magnitude of the imaginary component of the material dielectric constant. Materials with a small  $\epsilon''$  have a large, narrow absorption peak, whereas materials with a large  $\epsilon''$  have a small, broader absorption peak.<sup>31</sup>

The ratio of the real parts of  $\epsilon'_{\perp}/\epsilon'_{\parallel}$  does not oscillate with frequency and what is more, at the frequency of  $\omega \simeq \omega_{pl}$  exhibits the singularity. Thus, we demonstrate below the plots for  $\epsilon'_{\perp}(\omega)$  and  $\epsilon'_{\parallel}(\omega)$  separately.

Figure 2 shows the real part of the dielectric permeability components for Au nanoparticles as a function of normalized frequency, obtained by using Eqs. (32) and (35) in numerical calculations. The magnitude of  $\epsilon'$  reaches a minimum value at  $\omega \rightarrow 0$ , and  $\epsilon' \rightarrow 0$  at  $\omega \rightarrow \omega_{pl}$ . Among the two components of  $\epsilon'$ , the frequency dependence is more pronounced for the longitudinal one:  $\epsilon'_{\parallel}$  attains the smallest negative value at  $\omega \rightarrow 0$  in the case of the prolate Au nanoparticle and the maximal negative value for the oblate one. The absolute magnitude of both components of  $\epsilon'$  is essentially enhanced as the radius of the particle is increased (especially at  $\omega \rightarrow 0$ ).

Below, we will consider several approaches that enable us to derive the explicit analytical expressions for  $\sigma'$  and  $\sigma''$  from Eqs. (34) and (35).

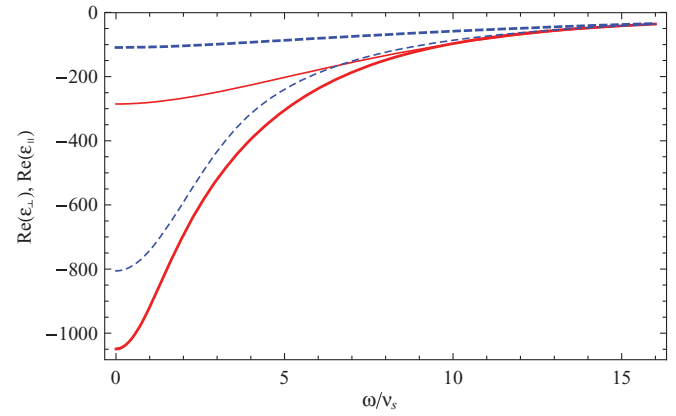


FIG. 2. (Color online) The dependence of  $\epsilon'_{\perp}, \epsilon'_{\parallel}$  for both the prolate ( $R_{\perp}/R_{\parallel} = 0.1$ , solid lines) and the oblate ( $R_{\perp}/R_{\parallel} = 10$ , dashed lines) Au particles (with  $R = 50 \text{ \AA}$ ) vs the frequency ratio  $\omega/\nu_s$ . Thick curves are for parallel components, and thin curves are for perpendicular components of  $\epsilon'$ .

## IV. LIMIT CASES: SIZE EFFECTS

### A. Frequency approach

The straightforward evaluations of the dielectric permeability of a single MN or its conductance can be made when the  $\Psi$  function entering in Eq. (23) or in Eqs. (34) and (35) takes the simplest form. Let us introduce the value

$$\nu_s = \frac{v'}{2R}, \quad (36)$$

which will characterize the frequency of electron collisions with the spherical MN surfaces and where  $R$  is the sphere radius. This allow us to rewrite Eq. (22) as

$$q = \frac{\nu}{\nu_s} - i \frac{\omega}{\nu_s}. \quad (37)$$

(i) First, we consider, for example, the case  $|q| \gg 1$ . In the frequency scale, this implies that both inequalities  $\nu \gg \nu_s$  and  $\omega \gg \nu_s$  must be executed. Then, Eq. (21) reduces to the form

$$\Psi(q)|_{|q| \gg 1} \approx \frac{4}{3} - \frac{2}{q} + \frac{4}{q^3} - \dots \quad (38)$$

Accounting for Eqs. (38) and (22), we can calculate approximately the real and imaginary parts of the ratio:

$$\text{Re} \left( \frac{\Psi(\theta)}{\nu - i\omega} \right)_{|q| \gg 1} \approx \frac{4}{3} \frac{\nu}{\nu^2 + \omega^2} - \frac{v'(\theta)}{R} \frac{\nu^2 - \omega^2}{(\nu^2 + \omega^2)^2} + \dots, \quad (39)$$

$$\text{Im} \left( \frac{\Psi(\theta)}{\nu - i\omega} \right)_{|q| \gg 1} \approx \frac{4}{3} \frac{\omega}{\nu^2 + \omega^2} - 2 \frac{v'(\theta)}{R} \frac{\nu \omega}{(\nu^2 + \omega^2)^2} + \dots, \quad (40)$$

which enter into Eqs. (34) and (35). Here the velocity  $v'(\theta)$  is given by Eq. (28). The formula (39) at  $\nu \rightarrow 0$  agrees with an earlier estimation given in Ref. 45.

Substituting Eq. (39) into Eq. (34), and Eq. (40) into Eq. (35) and using the values of the integrals  $I_{\parallel}$  and  $I_{\perp}$  given in the

Appendix, one obtains for the real and imaginary parts of the conductivity tensor components the expressions

$$\sigma'_{(\perp)}(\omega) \approx \frac{ne^2}{m} \left( \frac{v}{v^2 + \omega^2} - \frac{9}{2} v_s \frac{v^2 - \omega^2}{(v^2 + \omega^2)^2} I_{(\perp)} + \dots \right), \quad (41)$$

$$\sigma''_{(\perp)}(\omega) \approx \frac{ne^2}{m} \left( \frac{\omega}{v^2 + \omega^2} - 9v_s \frac{v\omega}{(v^2 + \omega^2)^2} I_{(\perp)} + \dots \right), \quad (42)$$

provided that the conditions  $v \gg v_s$ ,  $\omega \gg v_s$ , and  $v = v_F$  are satisfied. To meet the requirement of  $v \gg v_s$ , e.g., for an Au particle at 0 °C, it is necessary that its radius should be  $R \gg 400 \text{ \AA}$ . The first term in the parentheses in Eqs. (41) and (42) results from the integration over the angle

$$\int_0^{\pi/2} \left( \frac{\sin \theta \cos^2 \theta}{\frac{1}{2} \sin^3 \theta} \right) d\theta = \frac{1}{3}. \quad (43)$$

The second term in the parentheses in Eqs. (41) and (42) contains the integrals  $I$ , which account for the particle nonsphericity and do not depend on the frequency. The simplest result for  $\sigma$  can be obtained for a spherical MN, when the integrals  $I$  for different polarizations coincide with each other and are equal to 1/3 [see Eq. (A5)].

As one can see, the first term in the parentheses in Eqs. (41) and (42) describes the Drude-Sommerfeld results for a spherical particle, and the second one gives the first correction of the kinetic theory to the volume electron scattering, allowing us to account for an electron scattering from the surfaces of the nanoparticle as well. The calculations of the frequency dependencies of the ratio  $\epsilon''_{\perp}/\epsilon''_{\parallel}$  while employing Eqs. (33) and (41) (and the conditions mentioned therein) give results qualitatively similar to our previous numerical calculations [using Eqs. (33) and (34)], depicted in Fig. 1, though without any oscillations. But, quantitatively, the results obtained from Eq. (34) are of one or even two orders of magnitude lower (depending on the radius of MN) than those following from the Drude-Sommerfeld formula or from Eq. (41).

(ii) For the opposite limit case, when  $|q| \ll 1$  (or  $v \ll v_s$  and  $\omega \ll v_s$ ), we can take advantage of the expansion

$$e^{-q} \simeq 1 - q + \frac{q^2}{2!} - \frac{q^3}{3!} + \frac{q^4}{4!} - \frac{q^5}{5!} + \frac{q^6}{6!} - \dots,$$

and then from Eq. (21), we immediately obtain

$$\Psi(q)|_{|q| \ll 1} \approx \frac{1}{2}q - \frac{2}{15}q^2 + \frac{1}{36}q^3 - \dots \quad (44)$$

In this case, we can find for the real and imaginary parts of the above-mentioned ratio the relations

$$\text{Re} \left( \frac{\Psi(\theta)}{v - i\omega} \right)_{|q| \ll 1} \approx \frac{R}{v'(\theta)} - \frac{8}{15}v \left( \frac{R}{v'(\theta)} \right)^2 + \dots, \quad (45)$$

$$\text{Im} \left( \frac{\Psi(\theta)}{v - i\omega} \right)_{|q| \ll 1} \approx \frac{8}{15}\omega \left( \frac{R}{v'(\theta)} \right)^2 + \dots \quad (46)$$

This permits us to get for the  $\sigma$  components the following expressions:

$$\sigma'_{(\perp)} \approx \frac{9ne^2}{4m} \left( \frac{R}{v} I_{(\perp)}^<|_{v=v_F} - \frac{2}{15} \frac{v}{v_s^2} J_{(\perp)} + \dots \right), \quad (47)$$

$$\sigma''_{(\perp)}(\omega) \approx \frac{9}{30} \frac{ne^2}{m} \frac{\omega}{v_s^2} (J_{(\perp)} + \dots), \quad (48)$$

provided that  $v \ll v_s$ ,  $\omega \ll v_s$ , and  $v = v_F$ . In other words, the first condition means that the radius of MN should obey the condition  $R \ll v_F/(2v)$ . The first term in the parentheses of Eq. (47) is the result of the integration over angle  $\theta$  with  $v'(\theta)$  in the denominator [see Eqs. (A6) and (A7)], and the second one can be given by

$$J_{(\perp)} = \frac{1}{R^2} \frac{R_{\parallel}^2 R_{\perp}^2}{R_{\perp}^2 - R_{\parallel}^2} \left[ \pm \begin{pmatrix} 1 \\ 1/2 \end{pmatrix} \mp \begin{pmatrix} 1 \\ \frac{1}{2}(R_{\perp}/R_{\parallel})^2 \end{pmatrix} \right] \times \frac{R_{\parallel}}{\sqrt{R_{\perp}^2 - R_{\parallel}^2}} \arctan \frac{\sqrt{R_{\perp}^2 - R_{\parallel}^2}}{R_{\parallel}}. \quad (49)$$

The upper (lower) signs and upper (lower) symbols in the parentheses on the right-hand side of Eq. (49) correspond to those on the left-hand side of this equation. In the case of prolate spheroidal particles ( $R_{\parallel} > R_{\perp}$ ), one should make in Eq. (49) only the following replacement:

$$\arctan \frac{\sqrt{R_{\perp}^2 - R_{\parallel}^2}}{R_{\parallel}} \rightarrow \frac{1}{2i} \ln \left| \frac{R_{\parallel} - \sqrt{R_{\parallel}^2 - R_{\perp}^2}}{R_{\parallel} + \sqrt{R_{\parallel}^2 - R_{\perp}^2}} \right|, \quad (50)$$

and in the case of a spherical symmetric MN,  $R_{\parallel} = R_{\perp} \equiv R$ , and  $J_{\parallel} = J_{\perp} \equiv 1/3$ .

As one can see from Eq. (47), the real part of  $\sigma_{(\perp)}$  does not depend on the frequency, but only on the particle geometry, which is defined here by the parameters  $I^<$  and  $J$ . For the imaginary part of  $\sigma_{(\perp)}$ , we have from Eq. (48) the linear enhancement with the frequency. This implies that

$$\epsilon'_{(\perp)} \approx 1 - \frac{9}{30} \left( \frac{\omega_{pl}}{v_s} \right)^2 J_{(\perp)} \quad (51)$$

does not depend on the frequency, provided that the conditions  $\omega \ll v_s$  and  $v \ll v_s$  are fulfilled.

## B. Size approach

The cases of different relations between the particle sizes and the conduction electron mean free path inside a particle remain to be examined. Using Eq. (28), we can rewrite Eq. (22) in somewhat another form:

$$q = q_1(\theta) - iq_2(\theta), \quad (52)$$

with

$$q_1(\theta) = \frac{1}{\sqrt{\left(\frac{l}{2R_{\parallel}}\right)^2 \cos^2 \theta + \left(\frac{l}{2R_{\perp}}\right)^2 \sin^2 \theta}}, \quad (53)$$

where  $2R_{\parallel}$  is the length of the MN along the  $z$  axis, which is directed along the principal spheroid axis,  $2R_{\perp}$  is the MN size along the  $x$  or  $y$  directions,

$$l = \frac{v_F}{\nu} \quad (54)$$

has the sense of the length of an electron mean free path (for Au at  $0^\circ\text{C}$ , e.g.,  $l \simeq 410 \text{ \AA}$ ), and

$$q_2(\theta) = \frac{1}{\sqrt{\left(\frac{\nu_{s\perp}}{\omega}\right)^2 \sin^2 \theta + \left(\frac{\nu_{s\parallel}}{\omega}\right)^2 \cos^2 \theta}}. \quad (55)$$

Here

$$\nu_{s\parallel} = \frac{v_F}{2R_{\parallel}}, \quad \nu_{s\perp} = \frac{v_F}{2R_{\perp}} \quad (56)$$

are the frequencies of the electron collision with the particle surfaces along and across the  $z$  axis of a spheroid, respectively.

Let us consider the possible relations between  $l$  and particle sizes  $2R_{\parallel}$  and  $2R_{\perp}$ .

(i) The conduction electron mean free path is much less than the sizes of the particles along particular directions:  $l \ll 2R_{\perp}$ ,  $l \ll 2R_{\parallel}$ . As follows from Eq. (53),  $q_1(\theta)|_{\nu=v_F} \gg 1$ . In this case, an electron is scattered predominately inside the volume of MN. If, moreover,  $q_2 \rightarrow 0$ , i.e.,  $\nu_{s\parallel}, \nu_{s\perp} \gg \omega$ , then from Eq. (21), one gets

$$\Psi \simeq \frac{4}{3}. \quad (57)$$

Substituting Eq. (57) into Eqs. (34) and (35) and using Eq. (43), we obtain the Drude-Sommerfeld formulas for the real and imaginary parts of  $\sigma$ , presented above by the first term in the parentheses in Eqs. (41) and (42).

(ii) The mean free path of a conduction electron is much greater than the particle sizes along particular directions:  $l \gg 2R_{\perp}$ ,  $l \gg 2R_{\parallel}$ . In this case, an electron scattering occurs mainly from the inner surface of the MN. The electrons oscillate between the walls of the particle with different frequencies, including  $\nu_{s\parallel}$ ,  $\nu_{s\perp}$ . In accordance with Eq. (53), the inequality  $q_1(\theta) \ll 1$  holds only for  $q_1$ . The parameter  $q_2$  remains arbitrary. Formally, we can put  $q_1(\theta) \rightarrow 0$ , and for the real and imaginary parts of the  $\Psi$  function one finds

$$\text{Re } \Psi(q)|_{q_1 \rightarrow 0} = \frac{4}{3} + \frac{4}{q_2} \left( \cos q_2 - \frac{1}{q_2} \sin q_2 \right) \quad (58)$$

and

$$\text{Im } \Psi(q)|_{q_1 \rightarrow 0} = -\frac{2}{q_2} - \frac{4}{q_2^3} + \frac{4}{q_2^2} \left( \frac{1}{q_2} \cos q_2 + \sin q_2 \right). \quad (59)$$

Equations (58) and (59) allow us to fulfill the calculation of the real and the imaginary parts of the ratio  $\Psi/(\nu - i\omega)$ , as we have done before. Then, we obtain

$$\text{Re} \left[ \frac{\Psi(q)}{\nu - i\omega} \right]_{q_1 \rightarrow 0} = \frac{1}{\omega} \left[ \frac{2}{q_2} - \frac{4}{q_2^2} \sin q_2 + \frac{4}{q_2^3} (1 - \cos q_2) \right], \quad (60)$$

$$\text{Im} \left[ \frac{\Psi(q)}{\nu - i\omega} \right]_{q_1 \rightarrow 0} = \frac{4}{\omega} \left[ \frac{1}{3} + \frac{1}{q_2^2} \left( \cos q_2 - \frac{1}{q_2} \sin q_2 \right) \right]. \quad (61)$$

The parameter  $q_2$ , defined by Eq. (55), is governed by the frequency. Depending on the ratio between the incident frequency and the frequencies  $\nu_{s\parallel}$  and  $\nu_{s\perp}$ , the value of  $q_2$  can be greater or less than 1. This makes it difficult to perform subsequent analytical calculations of the integrals involved into Eqs. (34) and (35). Below, we examine some particular cases for which the calculations of  $\sigma$  are the most simple. It should be noted also that the corresponding expressions for the components of  $\epsilon$  can be easily obtained by substituting  $\sigma$  into Eqs. (32) and (33).

### 1. Conductivity of a spherical MN

In the case of a spherical MN there are three characteristic frequencies that are considered usually: the frequency of an incident electromagnetic field  $\omega$ , the collision frequency of electrons in the particle volume  $\nu$ , and the vibration frequency between the particle walls  $\nu_s$  (if the particle size is less than the electron mean free path). When  $\nu > \nu_s$ , the mechanism of an electron scattering in the bulk is dominated, and an electron scattering from the particle surface gives only small corrections of the order of  $\nu_s/\nu$ . But we are interested in the case when the mechanism of the surface electron scattering dominates, which corresponds to  $\nu < \nu_s$ .

For particles of a spherical shape, the electric conductivity becomes a scalar quantity, and one can put  $R_{\parallel} = R_{\perp} \equiv R$  in Eq. (27); then  $q$  and the  $\Psi$  function in Eqs. (25) and (26) are not dependent on the angle  $\theta$ . Accounting for Eq. (43), this makes it possible to obtain for  $\sigma$  the simple expression

$$\sigma_{sph}^c = \sigma_{\parallel}^c = \sigma_{\perp}^c = \frac{3ne^2}{4m} \frac{\Psi(q)}{\nu - i\omega} \Big|_{\nu=v_F}, \quad (62)$$

with  $q = 2R(\nu - i\omega)/v_F$ . To calculate  $\sigma_{sph}^c$ , one can use either Eqs. (39) and (40) or Eqs. (45) and (46) or Eqs. (60) and (61) for the different limit cases considered above. For example, we restrict ourselves here only to the case when  $\nu \ll \nu_s$ . In this limit case, to a first approximation, one can put  $q_1 \rightarrow 0$ . Then Eqs. (60) and (61) with  $q_2 = \omega/\nu_s$  can be used in Eq. (62). As a result, one obtains for the real and imaginary parts of  $\sigma$  the following expressions:

$$\sigma'_{sph} \simeq \frac{3}{8\pi} \nu_s \frac{\omega_{pl}^2}{\omega^2} \left[ 1 - \frac{2\nu_s}{\omega} \sin \frac{\omega}{\nu_s} + \frac{2\nu_s^2}{\omega^2} \left( 1 - \cos \frac{\omega}{\nu_s} \right) \right], \quad (63)$$

$$\sigma''_{sph} \simeq \frac{\omega_{pl}^2}{4\pi\omega} \left[ 1 + 3 \left( \frac{\nu_s}{\omega} \right)^2 \left( \cos \frac{\omega}{\nu_s} - \frac{\nu_s}{\omega} \sin \frac{\omega}{\nu_s} \right) \right], \quad (64)$$

provided that  $\nu \ll \nu_s$ , where  $\nu_s = v_F/(2R)$ . The last expression in the Drude-Sommerfeld approximation looks like<sup>14</sup>

$$\sigma''_{sph} = \frac{\omega}{4\pi} \frac{\omega_{pl}^2}{\nu^2 + \omega^2}. \quad (65)$$

If one puts the oscillation terms in Eqs. (63) and (64) equal to zero and uses Eqs. (32) and (33), then one obtains the expression for the real part of the dielectric function, which coincides with Eq. (1) at  $\nu \rightarrow 0$ , but for the imaginary part of the dielectric function, one gets Eq. (2) only if the

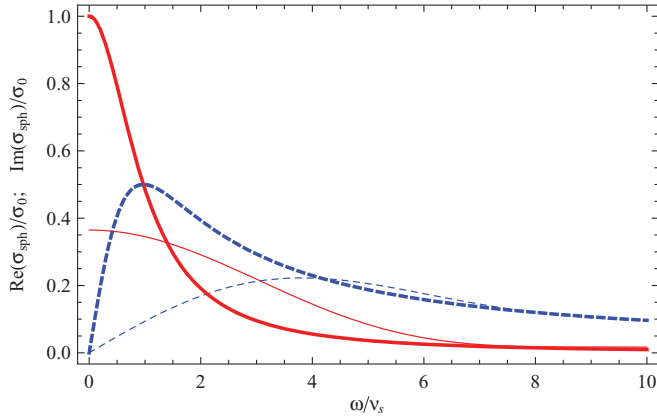


FIG. 3. (Color online) The real  $\sigma'$  (solid lines) and imaginary  $\sigma''$  (dashed lines) parts of the ratio of the electric conductivity to the static conductivity  $\sigma_0$  vs the frequency ratio for a spherical Au particle with  $R = 200$  Å. The thin lines correspond to the results obtained using the kinetic method, and the thick lines correspond to the Drude-Sommerfeld formulas.

replacement  $\nu \rightarrow 3\nu_s/2$  is done. This replacement is the same one as presented by Eq. (3), which has been often used in a phenomenological approximation.

The calculated results of the real and imaginary parts of an electric conductivity across the frequency normalized to  $\nu_s$  are shown in Fig. 3 for a spherical Au nanoparticle, obtained with the use of both the kinetic method and the Drude-Sommerfeld formulas. The conductivity is measured on the scale of the static conductivity  $\sigma_0 = ne^2/(m\nu)$ . For calculations of  $\sigma$ , Eqs. (34) and (35) have been used in the kinetic case, and Eqs. (2) and (65) have been used in the Drude-Sommerfeld case. For illustration, the numerical parameters for the Au particle<sup>44</sup> and  $\omega_{pl} = 1.37 \times 10^{16} \text{ s}^{-1}$  were chosen. As can be seen in Fig. 3, the kinetic method appreciably changes the frequency dependence of  $\sigma_{sph}$  at low frequencies, and at high frequencies ( $\omega \gg \nu_s$ ) it gives the same result for  $\sigma_{sph}$  as that which follows from the Drude-Sommerfeld formula. The difference between the kinetic and Drude-Sommerfeld results is enhanced markedly as the particle radius is decreased. The real part of  $\sigma$  is peaked at  $\omega/\nu_s \rightarrow 0$  in both cases, whereas the imaginary part of  $\sigma$  is peaked at  $\omega = \nu_s$  in the Drude-Sommerfeld case and at  $\omega \approx 4\nu_s$  using the kinetic method.

For an extremely low  $\omega \ll \nu_s$  or an extremely high  $\omega \gg \nu_s$  frequency, one can find from Eqs. (63) and (64), after some algebra, the next simple approximation for  $\sigma'$ ,

$$\sigma'_{sph} = \frac{3}{16\pi} \omega_{pl}^2 \begin{cases} \frac{R}{\nu_F}, & \omega \ll \nu_s, \\ \frac{\nu_F}{R\omega^2}, & \omega \gg \nu_s, \end{cases} \quad (66)$$

and for  $\sigma''$ ,

$$\sigma''_{sph} = \frac{\omega_{pl}^2}{4\pi} \begin{cases} \frac{\omega}{2} \left(\frac{R}{\nu_F}\right)^2, & \omega \ll \nu_s, \\ \frac{1}{\omega}, & \omega \gg \nu_s. \end{cases} \quad (67)$$

The results of Eqs. (66) and (67) at  $\omega \gg \nu_s$  correspond to those presented above by first terms in the square brackets in Eqs. (63) and (64), respectively.

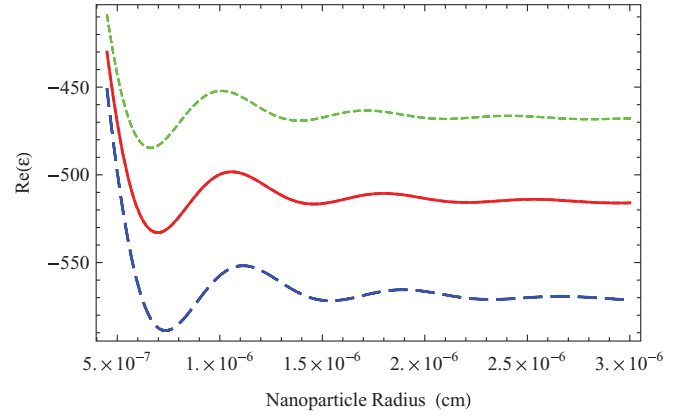


FIG. 4. (Color online) The dependence of  $\epsilon'$  for a spherical Au particle vs the radius  $R$  at the frequencies of  $\omega = 5.7 \times 10^{14} \text{ s}^{-1}$  (long-dashed line),  $6 \times 10^{14} \text{ s}^{-1}$  (solid line), and  $6.3 \times 10^{14} \text{ s}^{-1}$  (short-dashed line).

The calculations employing Eqs. (63) and (64) for an Au particle with  $R = 200$  Å give results similar qualitatively to the ones above presented, but quantitatively, they are at the  $\sigma$  maximum of approximately 30% higher.

In spite of the oscillation terms in square brackets in Eqs. (63) and (64), the ratios of both  $\sigma'_{sph}/\sigma_0$  and  $\sigma''_{sph}/\sigma_0$  do not oscillate with the frequency owing to the cutoff factors before these brackets.

Now, let us discuss shortly the dependence of the dielectric permeability on the size of MN. In Fig. 4, we present the results of our numerical calculations of  $\epsilon'(R)$  using Eqs. (32) and (35) at a fixed  $\omega$ . For illustration, we choose such frequencies from the frequency scale for which the above dependencies are the most pronounced for an Au particle.

The real  $\epsilon'$  and the imaginary  $\epsilon''$  parts of the dielectric permeability oscillate when the particle radius is increased (see Fig. 4 and Fig. 5). These oscillations have a damping character and practically vanish for MNs with high radii. The real part of  $\epsilon$  tends to +1, and the imaginary part tends to 0 at  $\omega \rightarrow 0$ . The real part has a first main minimum and the imaginary part has a first main maximum at small values of  $R$ . Both the minimum and the maximum of  $\epsilon$  are slightly shifted toward greater  $R$  with the frequency decreasing. In other words, this means that the resonance energy peak shifts toward the red side with increasing sizes of Au particles. The oscillation period in accordance with Eqs. (63) and (64) is defined by

$$T = \pi \frac{\nu_F}{R\omega} \quad (68)$$

and, as one can see, essentially depends on the product of  $R\omega$ . It becomes shorter at  $R\omega \ll \nu_F$ , and at  $R\omega \gg \nu_F$  it extends. Two types of oscillations may occur: at fixed  $\omega$  with varying  $R$  or at fixed  $R$  with changing  $\omega$ . For every fixed frequency there is a constant of  $\epsilon'$  or  $\epsilon''$  around which those quantities oscillate with altering  $R$ . At high frequencies, the period of oscillations is sharply decreased, and their amplitude is considerably lowered proportionally to the factors  $(\omega_{pl}/\omega)^2$  and  $\omega_{pl}^2/\omega$  before the square brackets in Eqs. (63) and (64), respectively.

If we assume that the dielectric function of the surrounding media  $\epsilon_m$  is close to unity, then for a spherical Au particle at a plasmon frequency  $\omega = \omega_{pl}/\sqrt{1 + 2\epsilon_m}$  we get the closely

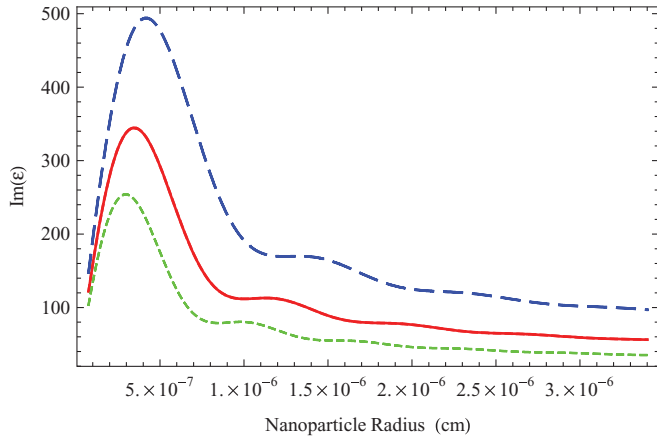


FIG. 5. (Color online) The dependence of  $\epsilon''$  for a spherical Au particle across the radius  $R$  at the frequencies of  $\omega = 5 \times 10^{14} \text{ s}^{-1}$  (long-dashed line),  $6 \times 10^{14} \text{ s}^{-1}$  (solid line), and  $7 \times 10^{14} \text{ s}^{-1}$  (short-dashed line).

packed oscillations of  $\epsilon'(R)$  within the amplitude interval  $-2 \div 1$ . The behavior of  $\sigma'(R)$  and  $\sigma''(R)$  at the frequencies  $\omega \ll \nu_s$  and  $\omega \gg \nu_s$  can be seen from Eqs. (66) and (67) as well.

## 2. Conductivity of an oblate MN

For oblate particles

$$l > 2R_{\perp} > 2R_{\parallel}. \quad (69)$$

We shall consider, for convenience, the frequency intervals  $\omega \ll \nu_{s,\perp}$  and  $\omega \gg \nu_{s,\parallel}$ . According to Eq. (55), the former interval corresponds to  $q_2|_{v=v_F} < 1$ , and the latter one corresponds to  $q_2|_{v=v_F} > 1$ . It is easy to show that Eqs. (60) and (61) for these frequency intervals transform to

$$\text{Re} \left[ \frac{\Psi(q)}{v - i\omega} \right]_{q_1 \rightarrow 0} \approx \frac{1}{\omega} \begin{cases} \frac{q_2}{2}, & \omega \ll \nu_{s,\perp}, \\ \frac{2}{q_2}, & \omega \gg \nu_{s,\parallel}, \end{cases} \quad (70)$$

$$\text{Im} \left[ \frac{\Psi(q)}{v - i\omega} \right]_{q_1 \rightarrow 0} \approx \frac{1}{\omega} \begin{cases} \frac{q_2^2}{6}, & \omega \ll \nu_{s,\perp}, \\ \frac{4}{3}, & \omega \gg \nu_{s,\parallel}. \end{cases} \quad (71)$$

Then, the integrals in Eqs. (34) and (35) can be calculated exactly in the approximations of (70) and (71), and for an arbitrary spheroid aspect ratio between  $R_{\parallel}$  and  $R_{\perp}$  we obtain the following expressions for the components of an electric conductivity:

$$\sigma'_{\perp}(\omega) \simeq \frac{9}{16\pi} \frac{\omega_{pl}^2}{\omega} \begin{cases} \frac{R\omega}{v_F} I_{\perp}(\parallel), & \omega \ll \nu_{s,\perp}, \\ \frac{v_F}{R\omega} I_{\perp}(\parallel), & \omega \gg \nu_{s,\parallel}. \end{cases} \quad (72)$$

$$\sigma''_{\perp}(\omega) \simeq \frac{1}{4\pi} \frac{\omega_{pl}^2}{\omega} \begin{cases} \frac{3}{2} \left( \frac{R\omega}{v_F} \right)^2 J_{\perp}(\parallel), & \omega \ll \nu_{s,\perp}, \\ 1, & \omega \gg \nu_{s,\parallel}. \end{cases} \quad (73)$$

In the case of  $\omega \ll \nu_{s,\perp}$ , Eq. (72) coincides with the first term found previously in Eq. (47), and in the case of  $\omega \gg \nu_{s,\parallel}$ , it coincides with the second term of Eq. (41) at  $\nu = 0$ . Similarly, Eq. (73) in the case of  $\omega \ll \nu_{s,\perp}$  agrees with the first term found previously in Eq. (48) with an accuracy of a numerical

coefficient, and in the case of  $\omega \gg \nu_{s,\parallel}$  it coincides with the first term of Eq. (42) at  $\nu = 0$ .

The above expressions can be transformed to their simplest forms for strongly deformed particles. Thus, for strongly oblate MNs, when  $R_{\perp} \gg R_{\parallel}$ , using Eqs. (A3) and (A9) from the Appendix, it can be easily found that at low frequencies

$$\left. \begin{aligned} \sigma'_{\parallel} &= \frac{9}{32\pi} \omega_{pl}^2 \frac{R_{\parallel}}{v_F} \\ \sigma'_{\perp} &= \sigma'_{\parallel} \left( \ln 2 \frac{R_{\perp}}{R_{\parallel}} - \frac{1}{2} \right) \end{aligned} \right\}, \quad \omega \ll \nu_{s,\perp}, \quad (74)$$

and at high frequencies

$$\left. \begin{aligned} \sigma'_{\parallel} &= \frac{9}{64\pi} \left( \frac{\omega_{pl}}{\omega} \right)^2 \frac{v_F}{R_{\parallel}} \\ \sigma'_{\perp} &= \sigma'_{\parallel} / 2 \end{aligned} \right\}, \quad \omega \gg \nu_{s,\parallel}. \quad (75)$$

Similarly, for  $\sigma''$  in the case of strongly oblate MNs at low frequencies, one gets

$$\left. \begin{aligned} \sigma''_{\parallel} &= \frac{3}{8\pi} \omega \left( \frac{\omega_{pl} R_{\parallel}}{v_F} \right)^2 \\ \sigma''_{\perp} &= \frac{1}{2} \sigma''_{\parallel} \left( \frac{R_{\perp}}{R_{\parallel}} \arctan \frac{R_{\perp}}{R_{\parallel}} - 1 \right) \end{aligned} \right\}, \quad \omega \ll \nu_{s,\perp}, \quad (76)$$

and at high frequencies one gets

$$\sigma'_{\perp} \equiv \sigma''_{\parallel} = \frac{\omega_{pl}^2}{4\pi\omega}, \quad \omega \gg \nu_{s,\parallel}. \quad (77)$$

It remains to consider how the optical properties of MNs evolve at  $\nu_{s,\perp} \leq \omega \leq \nu_{s,\parallel}$  between the low- and high-frequency intervals. This interval is just that for which the parameter  $q_2$  can be greater or less than 1. In this case, only the numerical evaluations of the integrals entered into Eqs. (34) and (35) can be performed. The obtained results for the real part of  $\sigma$  can be found in Ref. 45.

## 3. Conductivity of a prolate MN

For prolate particles

$$l > 2R_{\parallel} > 2R_{\perp}. \quad (78)$$

It is also worth noting that the approximations (70) and (71) still remain valid for the case of inequalities (78) if the transposition  $\nu_{s,\perp} \leftrightarrow \nu_{s,\parallel}$  is carried out in Eqs. (70) and (71). As a result, the integrals in Eqs. (34) and (35) can be easily calculated, and for prolate particles with an arbitrary aspect ratio of  $R_{\parallel}/R_{\perp}$ , one obtains results similar to the ones given by Eqs. (72) and (73), in which both replacements (50) and (A8) have been made for  $J$  and the integrals  $I, I^<$ . Below, we write down only the results for strongly prolate particles ( $R_{\parallel} \gg R_{\perp}$ ) at low and high frequencies. Using Eqs. (A4) and (A10), it is easy to find that

$$\left. \begin{aligned} \sigma'_{\parallel} &= \frac{9}{64} \omega_{pl}^2 \frac{R_{\parallel}}{v_F} \\ \sigma'_{\perp} &= \sigma'_{\parallel} / 2 \end{aligned} \right\}, \quad \omega \ll \nu_{s,\parallel}, \quad (79)$$

$$\left. \begin{aligned} \sigma'_{\parallel} &= \frac{9}{256} \left( \frac{\omega_{pl}}{\omega} \right)^2 \frac{v_F}{R_{\perp}} \\ \sigma'_{\perp} &= 3\sigma'_{\parallel} / 2 \end{aligned} \right\}, \quad \omega \gg \nu_{s,\perp}. \quad (80)$$

For  $\sigma''$ , just as for  $\sigma'$ , in the case of strongly prolate MNs, one finds

$$\left. \begin{aligned} \sigma_{\perp}'' &= \frac{3}{16\pi} \omega \left( \frac{\omega_{pl} R_{\perp}}{v_F} \right)^2 \\ \sigma_{\parallel}'' &= -2\sigma_{\perp}'' \left( 1 + \ln \frac{R_{\perp}}{2R_{\parallel}} \right) \end{aligned} \right\}, \quad \omega \ll v_{s,\parallel}, \quad (81)$$

and at high frequencies  $\omega \gg v_{s,\perp}$ , we have found  $\sigma_{\parallel}'' \simeq \sigma_{\perp}'' = \omega_{pl}^2 / (4\pi\omega)$ , which coincides exactly with Eq. (77) for oblate particles.

Comparing Eqs. (79)–(81) for a strongly prolate particle to the corresponding Eqs. (72)–(76) for a strongly oblate particle shows that the character of the frequency dependence of the corresponding components of the electric conductivity tensor remains practically the same. The behavior of this dependence resembles the asymptotic behavior of the Drude-Sommerfeld frequency dependence for an electron scattering in the volume of MN; this can be easily verified from the first summand on the right-hand sides of Eqs. (41) and (42) by setting  $\omega \ll v$  or  $\omega \gg v$ . The difference consists only in the fact that for electron scattering in the volume, the high-frequency conductivity close to the frequency  $\omega \approx v$  goes smoothly to the saturation. However, for the strongly asymmetric MNs there exists an entire transitional region between the minimum and the maximum transit rates where the frequency dependence of  $\sigma$  appreciably differs from the volume case.

In the case of the frequency interval  $v_{s,\parallel} \leq \omega \leq v_{s,\perp}$ , the numerical evaluations of the integrals involved in Eqs. (34) and (35) can be performed, and the obtained results for  $\sigma$  have been presented in Ref. 45.

## V. RESULTS AND DISCUSSION

One of the most important cases takes place for the frequencies  $\omega \gg v_s$ , with  $v_s = v_F / (2R) \gg v$ . In terms of  $q$  this corresponds to the situation when  $|q_1| \ll 1$  and  $|q_2| \gg 1$ . In this case, one may use expressions (58) and (59) at  $q_1 \rightarrow 0$  to obtain the results for an asymptotically high value of  $q_2$ . As a result, we get for the real and imaginary parts of an electric conductivity of a single spheroidal MN with an arbitrary aspect ratio of  $R_{\perp} / R_{\parallel}$  the following expressions:

$$\sigma'_{(\perp)}(\omega) \approx \frac{1}{4\pi} \left( \frac{\omega_{pl}}{\omega} \right)^2 \left( v + \frac{9}{4} \frac{v_F}{R} I_{(\perp)} + \dots \right), \quad (82)$$

$$\sigma''_{(\perp)}(\omega) \approx \frac{1}{4\pi} \left( \frac{\omega_{pl}}{\omega} \right)^2 \left( \omega - \frac{9}{4} \frac{v_F}{R} I_{(\perp)} + \dots \right), \quad (83)$$

provided that  $\omega \gg v_s \gg v$ . The parameters  $I_{\parallel}$  and  $I_{\perp}$  are given in the Appendix by Eqs. (A1) and (A2).

For a MN of a spherical shape these expressions take the simplest form

$$\sigma'_{(q_1 \ll 1, q_2 \gg 1)}(\omega) \simeq \frac{3}{8\pi} \left( \frac{\omega_{pl}}{\omega} \right)^2 v_s + \dots, \quad (84)$$

$$\sigma''_{(q_1 \ll 1, q_2 \gg 1)}(\omega) \simeq \frac{1}{4\pi} \left( \frac{\omega_{pl}}{\omega} \right)^2 \left( \omega - \frac{3}{2} v_s + \dots \right), \quad (85)$$

provided that  $\omega \gg v_s \gg v$ . The last formula demonstrates simply that the electron interaction with the surface of a spherical MN can shift the imaginary part of  $\sigma$  toward the

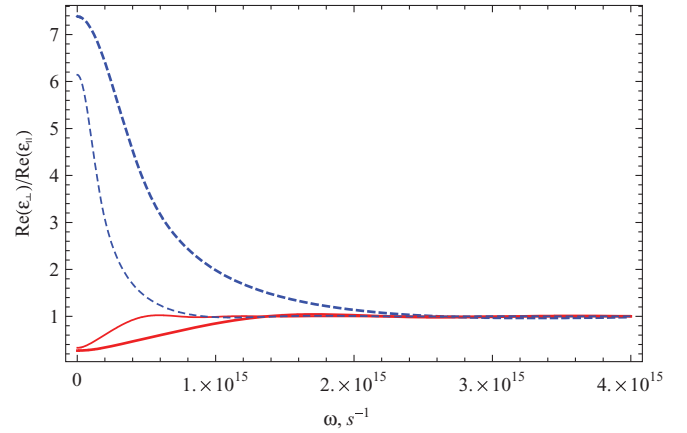


FIG. 6. (Color online) The frequency dependence of the reduced dielectric constant of Au particles with different  $R$  (Å): 50 (thick lines) and 150 (thin lines). Solid lines are for a prolate particle with  $R_{\perp}/R_{\parallel} = 0.1$ , and dashed lines are for an oblate one with  $R_{\perp}/R_{\parallel} = 10$ .

red side of the frequency scale. The smaller is the radius of the MN, the larger is the correction to the frequency shift.

Below, we will discuss the size dependence of the optical properties of MNs in more detail and will illustrate some results obtained in the sections above.

In Fig. 6, the results of numerical calculations of the ratio between the transversal and longitudinal components of the dielectric permeability versus the frequency are given for Au particles of different radii. The calculations were performed with the use of Eqs. (32) and (35) and the same numerical parameters as used above. At high frequencies ( $\omega \gg v_s$ ), the ratio of  $\epsilon'_{\perp} / \epsilon'_{\parallel} \rightarrow 1$  for different radii of Au particles. This result follows as well from Eqs. (32) and (73) at  $\omega \gg v_s$  for particles with an oblate shape and from Eqs. (32) and (77) for particles with a prolate shape. At low frequencies ( $\omega \ll v_s$ ), the particle size is strongly affected by the ratio of  $Re(\epsilon_{\perp}) / Re(\epsilon_{\parallel})$ . As can be seen in Fig. 6, the curves for MNs for prolate and oblate shapes merge into one as frequency grows, but for particles with a greater radii they merge at smaller frequencies.

The behavior of  $\epsilon'$  as a function of the ellipsoid aspect ratio  $R_{\perp} / R_{\parallel}$  at the frequency of a plasmon resonance in Au nanoparticles, embedded in the dielectric media with  $\epsilon_m = 1$ , is plotted in Fig. 7. The numerical calculations when employing Eqs. (32) and (35) were performed for two radii of a nanoparticle and for two light polarizations. As one can see in Fig. 7, the longitudinal component of  $\epsilon'$  in an oblate MN depends more strongly on the ratio  $R_{\perp} / R_{\parallel}$  than the transverse one. It becomes especially pronounced for Au nanoparticles (with  $R = 50$  Å) with small oblateness (e.g.,  $R_{\perp} / R_{\parallel} < 15$ ) when keeping the laser frequency fixed at  $\omega = \omega_{pl} / \sqrt{1 + 2\epsilon_m}$ : the oscillation magnitude of  $\epsilon'_{\perp}$  (around the constant of  $\epsilon' = -2$ ) becomes much larger than the ones for  $\epsilon'_{\parallel}$ . The amplitude of these oscillations is enhanced, and the period is extended as the ellipsoid aspect ratio  $R_{\perp} / R_{\parallel}$  increases. For MNs of greater radii, the number of oscillations is decreased, and their period is extended (compare the thin and thick curves in the Fig. 7 for Au particles with  $R = 50$  and 150 Å, for example). Both components of  $\epsilon'$  no longer

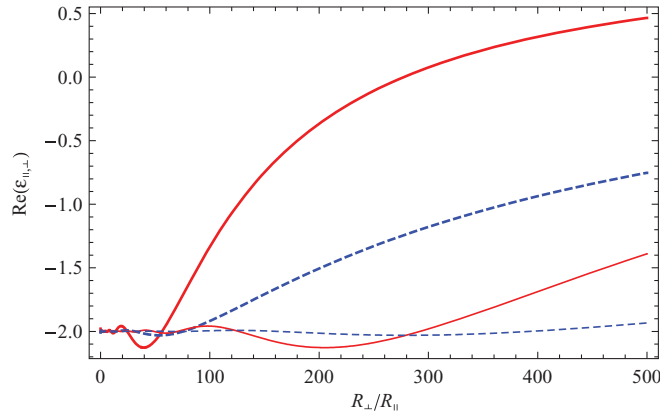


FIG. 7. (Color online) The dependence of the real part of the dielectric constant of Au particles with different  $R$  (Å), 50 (thick lines) and 150 (thin lines), on the ellipsoid aspect ratio at a frequency of plasmon resonance  $\omega = \omega_{pl}/\sqrt{3} \simeq 7.91 \times 10^{15} \text{ s}^{-1}$ . Solid lines are for the parallel component, and dashed lines are for the perpendicular component.

oscillate at high oblateness ( $R_{\perp}/R_{\parallel} > 80$ ) of Au particles with  $R = 50$  Å.

When the size of the particle is large enough, the parallel and perpendicular components of  $\epsilon'$  start to come together (see Fig. 2). For instance, at the frequency  $\omega \approx 6 \times 10^{14} \text{ s}^{-1}$  it takes place for Au particles with  $R = 130$  Å. At smaller frequencies it occurs for greater radii.

The presented dependencies display mainly the behavior of  $\epsilon'$  for an oblate nanoparticle ( $R_{\perp}/R_{\parallel} > 1$ ). In the case of a prolate nanoparticle ( $0 < R_{\perp}/R_{\parallel} < 1$ ), the numerical calculations employing Eqs. (32) and (35) for Au nanoparticles with a small size ( $\sim 50$  Å) at the frequency of the plasmon resonance give the oscillations of the transversal component of  $\epsilon'$ , the amplitude of which is enhanced, and the period is reduced as soon as the prolateness of the MN is increased. The longitudinal component of  $\epsilon'_{\parallel}$  oscillates in the prolate MN as well, but its amplitude is considerably smaller, and the period is much larger than the proper ones for  $\epsilon'_{\perp}$ .

The imaginary part of the dielectric function as a function of the ellipsoid aspect ratio  $R_{\perp}/R_{\parallel}$  is shown in Fig. 8. The numerical calculations were performed using Eqs. (33) and (34) at the plasmon frequency for two radii of nanoparticle and for two light polarizations. Since, for prolate MN, the value of  $\epsilon''$  practically does not depend on the spheroid aspect ratio  $R_{\perp}/R_{\parallel}$  (except for the case of a very high prolateness), in Fig. 8 we present only the results for an oblate MN. In contrast to the size behavior of  $\epsilon'$ , described above, one can see that the weak oscillations of  $\epsilon''$  hold together with linear increasing of  $\epsilon''$  just at small values of the aspect ratio  $R_{\perp}/R_{\parallel}$ . For Au particles, e.g., with  $R = 50$  Å, the weak oscillations of  $\epsilon''$  hold until  $R_{\perp}/R_{\parallel} < 150$  and is more sensible for the longitudinal component of  $\epsilon''$  than for the transversal one. Both components of  $\epsilon''$  reach the same maximum at some aspect ratios of  $R_{\perp}/R_{\parallel}$ , whose value depends on the radius of the particle. In the example depicted in Fig. 8 (for Au particles with  $R = 50$  Å), the values of  $\epsilon''_{\parallel} = \epsilon''_{\perp} \simeq 1.8$  have peaks at  $R_{\perp}/R_{\parallel} > 140$  for the parallel component and at  $R_{\perp}/R_{\parallel} \simeq 700$  for the perpendicular component of  $\epsilon''$ . Another interesting

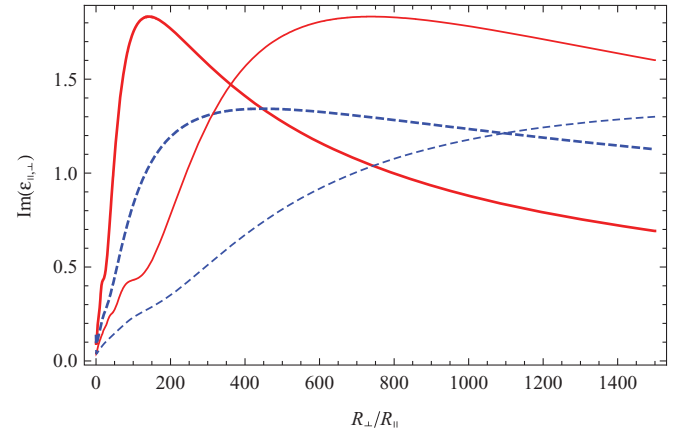


FIG. 8. (Color online) The dependence of the imaginary part of the dielectric constant of Au particles with different  $R$  (Å), 50 (thick lines) and 150 (thin lines), on the ellipsoid aspect ratio at the frequency of a plasmon resonance  $\omega \simeq 7.91 \times 10^{15} \text{ s}^{-1}$ . Solid lines are for the parallel component, and dashed lines are for the perpendicular component.

feature of the dependence of  $\epsilon''$  on  $R_{\perp}/R_{\parallel}$  is the intersection of curves for the parallel and perpendicular components for an oblate particle, as it takes place usually for particles with a spherical shape.

Finally, we illustrate how one may estimate the lifetime of surface plasmon excitation (or any others) in a MN using the above-derived formulas for  $\sigma$ . As follows from our previous calculations,<sup>21,39</sup> the linewidth can be represented as

$$\Gamma_{\beta}(\omega) = 4\pi L_{\alpha} \sigma_{\alpha\beta}(\omega), \quad (86)$$

where  $L_{\alpha}$  is defined after Eq. (6) and  $\sigma_{\alpha\beta}$  is the real part of the conductivity tensor, given by Eq. (23) for most general situations or by Eq. (34) for the spheroidal MN. For other particular cases, one may use for  $\text{Re } \sigma$  Eqs. (41), (47), (63), (66), (72), (74), (75), (79), (80), and (82). In particular, considering only the nanoparticles with a spherical shape ( $L = 1/3$ ) and restricting ourselves to the case  $v \ll v_s$ , we can choose Eq. (63) for illustration. Substituting it into Eq. (86), we obtain

$$\Gamma(\omega) \simeq \frac{\nu_F}{4R} \left( \frac{\omega_{pl}}{\omega} \right)^2 \left[ 1 - \frac{2v_s}{\omega} \sin \frac{\omega}{v_s} + \frac{2v_s^2}{\omega^2} \left( 1 - \cos \frac{\omega}{v_s} \right) \right]. \quad (87)$$

Taking into account only the first term in (87), we recover the well-known<sup>17,36,37</sup>  $1/R$  dependence of  $\Gamma$ :

$$\Gamma_0(\omega, R) = \frac{1}{4} \frac{\nu_F}{R} \left( \frac{\omega_{pl}}{\omega} \right)^2. \quad (88)$$

As seen from Eqs. (87) and (88), the lifetime ( $1/\Gamma$ ) of an excitation in the MN depends not only on the nanoparticle radius but also on the frequency (at which a given excitement is reasonable). For the frequency that corresponds to the excitation of a surface plasmon in MN in a vacuum,  $\omega = \omega_{pl}/\sqrt{3}$ , the following relation can be obtained from Eq. (88) in energy units:

$$\Gamma_0^{\text{SP}}(R) = \frac{3}{4} \frac{\nu_F}{R}. \quad (89)$$

The oscillating terms in Eq. (87) give rise to the oscillation of  $\Gamma$  around  $\Gamma_0$  as a function of both the particle radius and the frequency. They can be represented at the frequency of the surface plasmon as follows:

$$\Gamma_{\text{osc}}^{\text{SP}}(R) \simeq \frac{3\sqrt{3}}{4} \frac{\hbar}{\omega_{\text{pl}}} \left( \frac{v_F}{R} \right)^2 \times \left[ -\sin \frac{2R\omega_{\text{pl}}}{\sqrt{3} v_F} + \frac{\sqrt{3} v_F}{2R\omega_{\text{pl}}} \left( 1 - \cos \frac{2R\omega_{\text{pl}}}{\sqrt{3} v_F} \right) \right]. \quad (90)$$

The amplitude and period of oscillations can be estimated by the values

$$\Gamma_{\text{osc}}^{\text{max}} \simeq \frac{3\sqrt{3}\hbar v_F^2}{4\omega_{\text{pl}} R^2}, \quad T = \frac{\sqrt{3}\pi v_F}{R\omega_{\text{pl}}}, \quad (91)$$

respectively.

It is important to note that in the kinetic method this oscillatory behavior of  $\Gamma$  follows solely from the conditions of electron scattering on the nanoparticle surface.

Figure 9 shows the full linewidth  $\Gamma = \Gamma_0^{\text{SP}} + \Gamma_{\text{osc}}^{\text{SP}}$ , which is obtained by numerically evaluating Eqs. (89) and (90) for Na nanoparticles with the parameters<sup>44</sup>  $\omega_{\text{pl}} = 9.18 \times 10^{15} \text{ s}^{-1}$  and  $v_F = 1.07 \times 10^8 \text{ cm s}^{-1}$ . One can see that oscillating terms represent an important correction to  $\Gamma_0^{\text{SP}}(R)$  at small particle radii. Our result for Na nanoparticles only qualitatively agrees with similar results obtained in Refs. 37 and 38 since we try to apply the kinetic method to the range of  $R$  where the quantum effects (e.g., the Landau damping) play an important role. But, mostly, for the kinetics, the following inequality could be met:

$$R \gg \frac{2\pi\hbar}{m v_F}. \quad (92)$$

In order to study the significance of the oscillatory behavior in more general situations, it is necessary to perform the calculations of Eq. (86) using the real parts of Eqs. (23) or (34). This will be done separately.

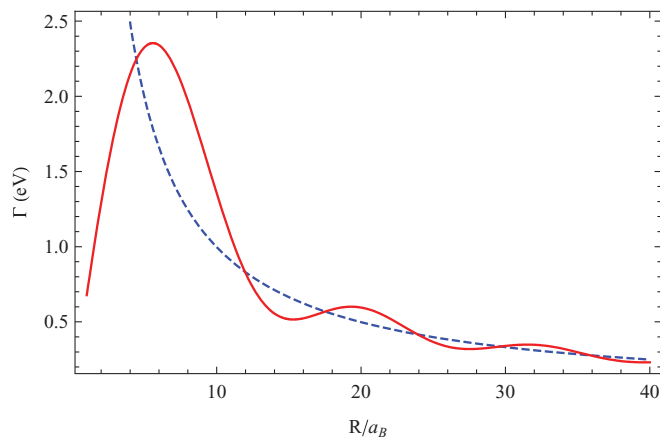


FIG. 9. (Color online) Linewidth  $\Gamma(R)$  of the surface plasmon resonance as a function of radius for Na nanoparticles in units of the Bohr radius  $a_B \simeq 0.53 \text{ \AA}$ . The smooth term  $\Gamma_0(R)$  is given by Eq. (89) (dashed line), and the solid line corresponds to the sum of Eqs. (89) and (90).

There are several experimental data for a dielectric constant of the powder of Ag and Al<sup>46</sup> and for Ag nanoparticles.<sup>47</sup> For a single Au particle we have found only the experimental data for an optical response.<sup>48</sup> A direct comparison of theoretical results with most of the available experimental measurements of the optical properties of MNs is still a matter of debate because inhomogeneities in nanoparticle size, shape, and local environment hide the homogeneous width of the surface plasmon resonance. There are very different data even for bulk permittivity of Au,<sup>49,50</sup> especially for its imaginary part.

## VI. CONCLUSIONS

The kinetic equation method is used to study the peculiarities of electron interactions with the surface of a spheroidal metal nanoparticle when the electron scattering from the particle surface becomes a dominant effect. Special attention was paid to studying the modification of the Drude-Sommerfeld model applied to the optical properties of MN. The real and imaginary parts of the dielectric permeability at the frequencies above and below the characteristic frequency of a free-electron passage between the walls of the particle were calculated for a single oblate and a prolate MN whose dimensions are much smaller than the wavelength of an electromagnetic wave.

It was established for spherical MNs that the kinetic method appreciably changes the frequency dependence of electrical conductivity at low frequencies, and at high frequencies ( $\omega \gg v_s$ ) it gives the same result as the one obtained from the Drude-Sommerfeld formula. Quantitatively, the results obtained by the kinetic method are of one or even two orders of magnitude lower (depending on the radius of MN) than those following from classical formulas. The difference between the results is enhanced markedly as the particle radius decreases, and the nanoparticle surface starts to play a more pronounced role.

The frequency dependencies of the components of the electric conductivity tensor  $\sigma$  were found, and their dependence on the spheroidal aspect ratio was investigated. Simple analytical expressions were found for this tensor in strongly oblate or prolate MNs at low and high frequencies.

The electron interaction with the surface of a spherical MN can shift the imaginary part of  $\sigma$  toward the red side of the frequency scale. The smaller the radius of the MN is, the greater the correction to the frequency shift is.

Two types of oscillations were established for small enough MNs: at fixed  $\omega$  with varying of  $R$  and at fixed  $R$  with changing  $\omega$ . These oscillations have a damping character and practically vanish otherwise at high frequencies or for MNs with high radii.

The ratio of  $\text{Im}(\epsilon_{\perp})/\text{Im}(\epsilon_{\parallel})$  oscillates with increasing frequency for both the prolate and the oblate MNs. In contrast, the ratio of the real parts  $\text{Re}(\epsilon_{\perp})/\text{Re}(\epsilon_{\parallel})$  does not oscillate with frequency. Together with that, the real  $\epsilon$  and the imaginary  $\epsilon$  parts of the dielectric permeability oscillate when the particle radius is increased. It was found that the particle size strongly affects the ratio  $\text{Re}(\epsilon_{\perp})/\text{Re}(\epsilon_{\parallel})$  at low frequencies ( $\omega \ll v_s$ ).

## ACKNOWLEDGMENT

The authors would like to thank E. A. Ponezha for her valuable comments and useful remarks.

## APPENDIX

Below we present the values for the integrals introduced in the Sec. IV.

$$I_{\parallel} = \frac{1}{\nu} \int_0^{\pi/2} \sin \theta \cos^2 \theta \nu'(\theta) d\theta = \frac{R}{8R_{\parallel}} \frac{2R_{\perp}^2 - R_{\parallel}^2}{R_{\perp}^2 - R_{\parallel}^2} - \frac{R}{8R_{\perp}} \frac{R_{\parallel}^3}{(R_{\perp}^2 - R_{\parallel}^2)^{3/2}} \ln \left| \frac{R_{\perp}}{R_{\parallel}} + \sqrt{\frac{R_{\perp}^2}{R_{\parallel}^2} - 1} \right|. \quad (\text{A1})$$

$$I_{\perp} = \frac{1}{\nu} \int_0^{\pi/2} \frac{1}{2} \sin^3 \theta \nu'(\theta) d\theta = \frac{3R}{16R_{\parallel}} - \frac{R}{16R_{\parallel}} \frac{R_{\perp}^2}{R_{\perp}^2 - R_{\parallel}^2} + \frac{R}{4R_{\perp}} \frac{R_{\parallel}}{\sqrt{R_{\perp}^2 - R_{\parallel}^2}} \left( 1 + \frac{R_{\parallel}^2}{4(R_{\perp}^2 - R_{\parallel}^2)} \right) \times \ln \left| \frac{R_{\perp}}{R_{\parallel}} + \sqrt{\frac{R_{\perp}^2}{R_{\parallel}^2} - 1} \right|. \quad (\text{A2})$$

For strongly oblate or prolate MNs, using the Eqs. (A1) and (A2), it is easy to find that

$$I_{(\perp), R_{\perp} \gg R_{\parallel}} \simeq \frac{1}{4} \frac{R}{R_{\parallel}} \left\{ \begin{array}{l} 1 \\ 1/2 \end{array} \right\}, \quad (\text{A3})$$

$$I_{(\perp), R_{\perp} \ll R_{\parallel}} \simeq \frac{\pi}{16} \frac{R}{R_{\perp}} \left\{ \begin{array}{l} 1 \\ 3/2 \end{array} \right\}, \quad (\text{A4})$$

respectively, and in the limit case of  $R_{\perp} = R_{\parallel} \equiv R$ , one gets

$$\lim_{R_{\parallel} \rightarrow R_{\perp}} I_{\parallel} = \lim_{R_{\parallel} \rightarrow R_{\perp}} I_{\perp} = \frac{1}{3}. \quad (\text{A5})$$

We advance here as well another typical integral that one meets when calculating  $\sigma$ .

$$I_{\parallel}^{\leq} = \nu \int_0^{\pi/2} \frac{\sin \theta \cos^2 \theta}{\nu'(\theta)} d\theta = \frac{R_{\parallel} R_{\perp}}{2R(R_{\perp}^2 - R_{\parallel}^2)} \times \left[ R_{\perp} - \frac{R_{\parallel}^2}{\sqrt{R_{\perp}^2 - R_{\parallel}^2}} \ln \left| \frac{R_{\perp}}{R_{\parallel}} + \sqrt{\frac{R_{\perp}^2}{R_{\parallel}^2} - 1} \right| \right], \quad (\text{A6})$$

$$I_{\perp}^{\leq} = \nu \int_0^{\pi/2} \frac{\sin^3 \theta}{2\nu'(\theta)} d\theta = -\frac{R_{\parallel} R_{\perp}^2}{4R(R_{\perp}^2 - R_{\parallel}^2)} + \frac{R_{\parallel} R_{\perp} (2R_{\perp}^2 - R_{\parallel}^2)}{4R(R_{\perp}^2 - R_{\parallel}^2)^{3/2}} \ln \left| \frac{R_{\perp}}{R_{\parallel}} + \sqrt{\frac{R_{\perp}^2}{R_{\parallel}^2} - 1} \right|. \quad (\text{A7})$$

In the case of prolate particles ( $R_{\parallel} > R_{\perp}$ ), one should perform in Eqs. (A1) and (A2) and in Eqs. (A6) and (A7) the following replacement:

$$\frac{1}{i} \ln \left| \frac{R_{\perp}}{R_{\parallel}} + i \sqrt{1 - \frac{R_{\perp}^2}{R_{\parallel}^2}} \right| \rightarrow \arcsin \sqrt{1 - \frac{R_{\perp}^2}{R_{\parallel}^2}}. \quad (\text{A8})$$

For strongly oblate or prolate MNs ( $R_{\perp} \gg R_{\parallel}$ ), using Eqs. (A6) and (A7), it is easy to obtain that

$$I_{(\perp), R_{\perp} \gg R_{\parallel}}^{\leq} \simeq \frac{1}{2} \frac{R_{\parallel}}{R} \left\{ \begin{array}{l} 1 \\ \ln 2 \frac{R_{\perp}}{R_{\parallel}} - 1/2 \end{array} \right\}, \quad (\text{A9})$$

$$I_{(\perp), R_{\perp} \ll R_{\parallel}}^{\leq} \simeq \frac{\pi}{4} \frac{R_{\perp}}{R} \left\{ \begin{array}{l} 1 \\ 1/2 \end{array} \right\}, \quad (\text{A10})$$

respectively, and in the limit case of  $R_{\perp} = R_{\parallel} \equiv R$ , one finds from Eqs. (A6) and (A7)

$$\lim_{R_{\parallel} \rightarrow R_{\perp}} I_{\parallel}^{\leq} = \lim_{R_{\parallel} \rightarrow R_{\perp}} I_{\perp}^{\leq} = \frac{1}{3}. \quad (\text{A11})$$

\*nrigor@bitp.kiev.ua

†ptomchuk@iop.kiev.ua

<sup>1</sup>J. Zhao, L. J. Sherry, G. C. Schatz, and R. P. Van Duyne, *IEEE J. of Selected Topics in Quantum Electronics* **14**, 1418 (2008).

<sup>2</sup>P. Alivisatos, *Nat. Biotechnol.* **22**, 51 (2004).

<sup>3</sup>E. Osbay, *Science* **311**, 189 (2006); D. Boyer, P. Tamarat, A. Maali, B. Lounis, and M. Orrit, *ibid.* **297**, 1160 (2002).

<sup>4</sup>T. Nagao, G. Han, C. V. Hoang, J.-S. Wi, A. Pucci, D. Weber, F. Neubrech, V. M. Silkin, D. Ender, O. Saito, and M. Rana, *Sci. Technol. Adv. Mater.* **11**, 054506 (2010).

<sup>5</sup>Y. B. Zheng, Y.-W. Yang, L. Jensen, L. Fang, B. K. Juluri, A. H. Flood, P. S. Weiss, J. F. Stoddart, and T. J. Huang, *Nano Lett.* **9**, 819 (2009).

<sup>6</sup>P. Bharadway, B. Deutsh, and L. Novotny, *Adv. Opt. Photonics* **1**, 438 (2009).

<sup>7</sup>N. L. Rosi and C. A. Mirkin, *Chem. Rev.* **105**, 1547 (2005).

<sup>8</sup>G. V. Hartland, *Annu. Rev. Phys. Chem.* **57**, 403 (2006).

<sup>9</sup>W. A. de Heer, *Rev. Mod. Phys.* **65**, 611 (1993).

<sup>10</sup>W. P. Halperin, *Rev. Mod. Phys.* **58**, 533 (1986).

<sup>11</sup>J. A. A. J. Perenboom, P. Wider, and F. Meier, *Phys. Rep.* **78**, 173 (1981).

<sup>12</sup>V. V. Klimov, *Nanoplasmonics* (Nauka, Moscow, 2010).

<sup>13</sup>L. Novotny and B. Hecht, *Principles of Nano-optics* (Cambridge University Press, Cambridge, 2006).

<sup>14</sup>C. F. Bohren and D. R. Huffman, *Absorption and Scattering of Light by Small Particles* (Wiley, Weinheim, 2004).

<sup>15</sup>U. Kreibig and M. Vollmer, *Optical Properties of Metal Clusters* (Springer, Berlin, 1995).

<sup>16</sup>A. Sommerfeld and H. Bethe, *Elektronentheorie der Metalle* (Springer, Heilderberg, 1933).

<sup>17</sup>A. Kawabata and R. Kubo, *J. Phys. Soc. Jpn.* **21**, 1765 (1966).

<sup>18</sup>S. Link and M. A. El-Sayed, *J. Phys. Chem. B* **103**, 4212 (1999).

<sup>19</sup>K. L. Kelly, E. Coronado, L. L. Zhao, and G. C. Schatz, *J. Phys. Chem. B* **107**, 668 (2003).

<sup>20</sup>E. S. Kooij and B. Poelsema, *Phys Chem Chem Phys* **8**, 3349 (2006).

<sup>21</sup>P. M. Tomchuk and N. I. Grigorchuk, *Phys. Rev. B* **73**, 155423 (2006).

<sup>22</sup>C. Noguez, *J. Phys. Chem. C* **111**, 3806 (2007).

<sup>23</sup>G. Mie, *Ann. Phys. (Weinheim, Germany.)* **25**, 377 (1908).

<sup>24</sup>J. C. Maxwell-Garnett, *Philos. Trans. R. Soc. London* **203**, 385 (1904); **205**, 237 (1906).

<sup>25</sup>P. Drude, *Ann. Phys. (Weinheim, Germany.)* **1**, 566 (1900).

- <sup>26</sup>R. H. Doremus, *J. Chem. Phys.* **40**, 2389 (1964); **42**, 414 (1965).
- <sup>27</sup>S. Stagira, M. Nisoli, S. De Silvestri, A. Stella, P. Tognini, P. Cheyssac, and R. Kofman, *Chem. Phys.* **251**, 259 (2000).
- <sup>28</sup>A. Arbouet, D. Christofilos, N. Del Fatti, F. Vallée, J.-R. Huntzinger, L. Arnaud, P. Billaud, and M. Broyer, *Phys. Rev. Lett.* **93**, 127401 (2004).
- <sup>29</sup>S. Berciaud, L. Cognet, P. Tamarat, and B. Lounis, *Nano Lett.* **5**, 515 (2005).
- <sup>30</sup>F. Hao and P. Nordlander, *Chem. Phys. Lett.* **489**, 141 (2007); N. K. Grady, N. J. Halas, and P. Nordlander, *ibid.* **399**, 167 (2004).
- <sup>31</sup>N. Harris, M. J. Ford, P. Mulvaney, and M. B. Cortie, *Gold Bull.* **41**, 5 (2008); L. Cognet and B. Lounis, *ibid.* **41**, 139 (2008).
- <sup>32</sup>V. M. Rentería and J. García-Macedo, *Colloids Surf. A* **278**, 1 (2006).
- <sup>33</sup>M. Hu, C. Novo, A. Funston, H. Wang, H. Staleva, S. Zou, P. Mulvaney, Y. Xia, and G. V. Hartland, *J. Mater. Chem.* **18**, 1949 (2008).
- <sup>34</sup>W. A. Kraus and G. C. Schatz, *J. Chem. Phys.* **79**, 6130 (1983).
- <sup>35</sup>M. M. Alvarez, J. T. Khoury, T. G. Schaaff, M. N. Shafiqullin, I. Vezmar, and R. L. Whetten, *J. Phys. Chem. B* **101**, 3706 (1997).
- <sup>36</sup>C. Yannouleas and R. A. Broglia, *Ann. Phys. (NY)* **217**, 105 (1992).
- <sup>37</sup>R. A. Molina, D. Weinmann, and R. A. Jalabert, *Phys. Rev. B* **65**, 155427 (2002).
- <sup>38</sup>G. Weick, R. A. Molina, D. Weinmann, and R. A. Jalabert, *Phys. Rev. B* **72**, 115410 (2005).
- <sup>39</sup>N. I. Grigorchuk and P. M. Tomchuk, *Phys. Rev. B* **80**, 155456 (2009).
- <sup>40</sup>J. A. Osborn, *Phys. Rev.* **67**, 351 (1945).
- <sup>41</sup>L. D. Landau and E. M. Lifshits, *Electrodynamics of Continuous Media* (Pergamon, New York, 1984).
- <sup>42</sup>C. Cercignani, *Theory and Application of the Boltzmann Equation* (Scottish Academic, Edinburgh, 1975); A. F. Alexandrov, L. C. Bogdankevich, and A. A. Rukhadze, *Principles of Plasma Electrodynamics* (Springer, Berlin, 1984).
- <sup>43</sup>S. V. Berezkina, I. A. Kuznetsova, and A. A. Yushmanov, *Zh. Tekh. Fiz.* **74**, 67 (2004).
- <sup>44</sup>C. Kittel, *Introduction to Solid State Physics*, 6th ed. (Wiley, New York, 1986).
- <sup>45</sup>N. I. Grigorchuk and P. M. Tomchuk, *Low Temp. Phys.* **33**, 341 (2007).
- <sup>46</sup>J. H. Liu, C. L. Chen, H. T. Lue, and J. T. Lue, *Meas. Sci. Technol.* **13**, 2032 (2002).
- <sup>47</sup>V. P. Drachev, U. K. Chettiar, A. V. Kildishev, H.-K. Yuan, W. Chai, and V. M. Shalaev, *Opt. Express* **16**, 1186 (2008).
- <sup>48</sup>N. Del Fatti, D. Christofilos, and F. Vallée, *Gold Bull.* **41**, 147 (2008).
- <sup>49</sup>P. Johnson and R. Christy, *Phys. Rev. B* **6**, 4370 (1972).
- <sup>50</sup>M. J. Weber, *Handbook of Optical Materials* (CRC, New York, 2003).